

Analysis of interchannel crosstalk in multimode parallel optical waveguides using the beam propagation method

Takuya Kudo^{1,*} and Takaaki Ishigure^{1,2}

¹Graduate School of Science and Technology, Keio University, 3-14-1 Hiyoshi, Kohoku-ku, Yokohama, 223-8522, Japan

²ishigure@appi.keio.ac.jp
taku87@z6.keio.jp

Abstract: We theoretically analyze the origin of inter-channel crosstalk in densely aligned multimode parallel optical waveguides for on-board interconnects using the Beam Propagation Method. In this paper, we demonstrate that the inter-channel crosstalk due to mode coupling is very low in graded-index (GI) circular-core waveguides because the propagation constants of the propagating modes are discrete. Additionally, it is also found that the waveguides with GI-type circular cores is sensitive to the optical confinement in the cladding: low-power cladding modes largely decrease the mode conversion.

©2014 Optical Society of America

OCIS codes: (230.7370) Waveguides; (250.5460) Polymer waveguides; (200.4650) Optical interconnects; (060.2270) Fiber characterization.

References and links

1. F. E. Doany, C. L. Schow, B. G. Lee, R. A. Budd, C. W. Baks, C. K. Tsang, J. U. Knickerbocker, R. Dangel, B. Chan, H. Lin, C. Carver, J. Huang, J. Berry, D. Bajkowski, F. Libsch, and J. A. Kash, "Terabit/s-class optical PCB links incorporating 360-Gb/s bidirectional 850 nm parallel optical transceivers," *J. Lightwave Technol.* **30**(4), 560–571 (2012).
 2. R. Dangel, C. Berger, R. Beyeler, L. Dellmann, M. Gmur, R. Hamelin, F. Horst, T. Lamprecht, T. Morf, S. Oggioni, M. Spreafico, and B. J. Offrein, "Polymer-waveguide-based board-level optical interconnect technology for datacom applications," *IEEE Trans. Adv. Packag.* **31**(4), 759–767 (2008).
 3. Y. Takeyoshi and T. Ishigure, "High-density 2 x 4 channel polymer optical waveguide with graded-index circular cores," *J. Lightwave Technol.* **27**(14), 2852–2861 (2009).
 4. H.-H. Hsu, Y. Hirobe, and T. Ishigure, "Fabrication and inter-channel crosstalk analysis of polymer optical waveguides with W-shaped index profile for high-density optical interconnections," *Opt. Express* **19**(15), 14018–14030 (2011).
 5. N. Bamiedakis, J. Beals, R. V. Penty, I. H. White, J. V. DeGroot, and T. V. Clapp, "Cost-effective multimode polymer waveguides for high-speed on-board optical interconnects," *IEEE J. Quantum Electron.* **45**(4), 415–424 (2009).
 6. M. Koshiba, K. Saitoh, and Y. Kokubun, "Heterogeneous multi-core fibers: proposal and design principle," *IEICE Electron. Express* **6**(2), 98–103 (2009).
 7. S. Jungling and J. C. Chen, "A study and optimization of eigenmode calculations using the imaginary-distance beam-propagation method," *IEEE J. Quantum Electron.* **30**(9), 2098–2105 (1994).
 8. T. Ishigure, M. Satoh, O. Takanashi, E. Nihei, T. Nyu, S. Yamazaki, and Y. Koike, "Formation of the refractive index profile in the graded index polymer optical fiber for gigabit data transmission," *J. Lightwave Technol.* **15**(11), 2095–2100 (1997).
 9. T. Kudo and T. Ishigure, "Analysis of inter-channel crosstalk in multi-mode parallel optical waveguide using beam propagation method," in *Proc. of IEEE Components, Packaging and Manufacturing Technology Symposium*, Japan (2012).
 10. T. Ishigure, Y. Koike, and J. W. Fleming, "Optimum index profile of the perfluorinated polymer-based GI polymer optical fiber and its dispersion properties," *J. Lightwave Technol.* **18**(2), 178–184 (2000).
 11. M. J. Adams, D. N. Payne, and F. M. E. Sladen, "Length-dependent effects due to leaky modes on multimode graded-index optical fibres," *Opt. Commun.* **17**(2), 204–209 (1976).
-

1. Introduction

In recent years, intensive efforts have been made to improve the efficiency of high-performance computers (HPCs) all over the world. Toward peta-flop scale and beyond, low-power consumption, high-bandwidth-density, and low-cost optical interconnect technologies are drawing much attention. Currently, further attention is concentrated on the chip-to-chip data exchange realized with multimode polymer parallel optical waveguides integrated on printed circuit boards (PCBs) [1]. Even in such optical waveguides, narrower channel pitch has been an important requirement [2] over the couple of years for much higher density wirings, and thus, the inter-channel crosstalk even in optical waveguides is a concern.

We have experimentally demonstrated that graded-index (GI) core polymer waveguides dramatically reduce the inter-channel crosstalk, compared to conventional step-index (SI) core waveguides [3–5]. However, the detailed mechanisms of inter-channel crosstalk in such multimode short-length waveguides have not yet been clarified. In this paper, we theoretically analyze the origin of inter-channel crosstalk in high-density multimode short-length parallel optical waveguides for on-board interconnects.

2. Coupled power theories of multi-mode waveguides

One of the origins of the inter-channel crosstalk in optical waveguides is known as mode coupling, which is a resonance of lightwave. In this section, we briefly introduce the theory of mode coupling. In general, mode coupling has been used for explaining the origin of inter-channel crosstalk in *single-mode multi-core* fibers (MCFs) [6].

2.1 Coupled power theory for single-mode waveguides

In the coupled power theory for dual-core single-mode waveguides (channel 1 and channel 2), the crosstalk due to mode coupling can be estimated from the power conversion efficiency η , shown by Eq. (1) [6].

$$\eta = \frac{1}{1 + \left(\frac{\beta_2 - \beta_1}{2\kappa} \right)^2} \quad (1)$$

Here, κ is the coupling constant which depends on the overlap integral of the electric fields of the propagating mode in channel 1 and channel 2, and β_1 and β_2 are the propagation constants of the propagating mode in channel 1 and channel 2, respectively; they are eigenvalues featuring each propagating mode. If channel 1 and channel 2 have identical structure, the mode coupling efficiency increases to 1.0, because β_1 and β_2 are identical. On the other hand, if channel 1 and channel 2 have slightly different structures, the mode coupling efficiency could decrease dramatically due to the difference in propagation constants, β_1 and β_2 .

2.2 Mode coupling in multi-mode waveguides

In multi-mode waveguides, the propagated lightwave is expanded to eigenfunctions described by Eq. (2):

$$E = \sum_m \phi_m \exp[i\beta_m z] \quad (2)$$

Here, E is the electric field, m is the mode number, β_m is the field amplitude, and z is the propagation distance. To calculate the distribution of the propagation constants for all the modes in multimode waveguides, we use the imaginary distance beam propagation method (ID-BPM) [8]. In ID-BPM the propagation length is replaced for $\tau = iz$, so Eq. (2) is rewritten as follows:

$$E = \sum_m \phi_m \exp[\beta_m \tau] \quad (3)$$

The exponential term in Eq. (2) is replaced for the exponential growth in Eq. (3), with the growth rate of each mode being equal to its real propagation constant. We calculate the distribution of the propagation constant in SI-square and GI-circular cores defined by Eq. (4), and GI-square core defined by Eq. (5) [9].

$$n(x, y) = \begin{cases} n_1 \left[1 - 2\Delta \left(\frac{(x^2 + y^2)^{\frac{1}{2}}}{a} \right)^g \right]^{\frac{1}{2}} & 0 \leq (x^2 + y^2)^{\frac{1}{2}} \leq a \\ n_1 [1 - 2\Delta]^{\frac{1}{2}} & a \leq (x^2 + y^2)^{\frac{1}{2}} \end{cases} \quad (4)$$

$$n(x, y) = \begin{cases} n_1 \left[1 - 2\Delta \left(\left| \frac{x}{a} \right|^g + \left| \frac{y}{a} \right|^g - \left| \frac{xy}{a^2} \right|^g \right) \right]^{\frac{1}{2}} & 0 \leq \left(\left| \frac{x}{a} \right|^g + \left| \frac{y}{a} \right|^g - \left| \frac{xy}{a^2} \right|^g \right) \leq 1 \\ n_1 [1 - 2\Delta]^{\frac{1}{2}} & \text{otherwise} \end{cases} \quad (5)$$

$$\Delta = \frac{n_1^2 - n_2^2}{2n_1^2} \quad (6)$$

Here, x and y are the orthogonal coordinates with the origin located at the center of the cores, Δ is the relative refractive index difference defined by Eq. (6), n_1 is the highest refractive index value in the core region (normally at the core center), n_2 is the cladding index, a is the core radius or half-width and half-height of square core, and g is the index exponent indicated in [9].

Figure 1 shows the distribution of the propagation constant in the SI-square, GI-circular, and GI-square cores. In Fig. 1, the vertical axis shows the normalized propagation constant b_m described by Eq. (7) with propagation constant β_m of the m -th mode number.

$$b_m = \frac{\beta_m - \min \beta}{\max \beta - \min \beta} \quad (7)$$

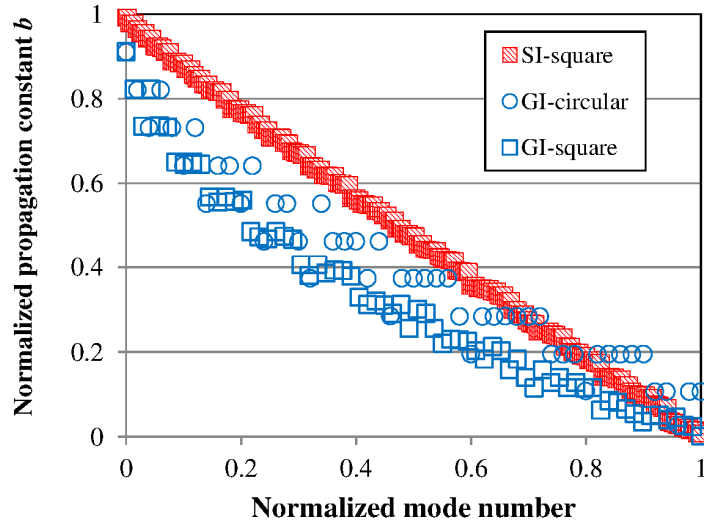


Fig. 1. The distribution of normalized propagation constants [9] ($2a = 35.0 \mu\text{m}$, $n_1 = 1.50$, $n_2 = 1.49$, $g = 2.0$).

Figure 1 indicates that the effective index is clearly discrete in the GI-type circular core, while the other two cores show continuous distribution of the propagation constant. The continuous distribution particularly for modes ranging from mode number 0.3 to 1 shown in the GI-type square core is attributed to the tail in the index profile [10]. Figure 2 shows the supposed index profile of the GI-square core approximated by Eq. (5). As shown in Fig. 2(b), the profile along the diagonal axis exhibits a tail near the core-cladding boundary.

Mode coupling in two-channel multimode parallel waveguides is considered as a superposition of mode coupling between each mode in the two cores. Here, when a particular mode in Ch. 1 has the same propagation constant as the corresponding mode in Ch. 2, the power conversion efficiency between these two modes is high, as discussed in the case of single-mode waveguides. Hence, from the results in Fig. 1, even if the two cores do not have identical structure, in SI-type square or GI-type square waveguides, there is a high probability that the propagation constant of a mode in Ch. 1 almost coincides with the propagation constant of a mode in Ch. 2 with different mode number, as illustrated in Fig. 3(a). Here, Ch. 1 and Ch. 2 are assumed to have slightly different structures, and thus, the propagation constant of the modes (from 2nd order to 6th order) in Ch. 1 are different from those in Ch. 2. However, the propagation constant of the modes from 2nd to 6th orders in Ch. 1 could coincide with those of 1st to 5th in Ch. 2. This is because the distributions of the propagation constant in Ch. 1 and Ch. 2 are continuous in the cases of SI-type and GI-type square cores. On the other hand, a slight structural difference in the GI-type circular core in Ch. 1 and 2 exhibits different distributions of propagation constant. In this case, as shown in Fig. 3(b), the probability in mismatching the propagation constants of the modes in the two cores are very high, because the propagation constants are discrete. Therefore, from the probability point of view, in waveguides with GI-type circular cores, the crosstalk due to mode coupling can be lower than in the SI-type square or GI-type square cores. The crosstalk in SI- and GI-core multimode waveguides are actually simulated in the following sections.

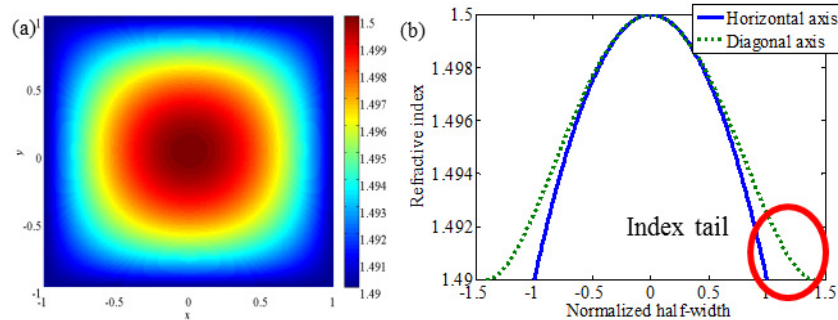


Fig. 2. Index-profile of GI-type square core ($n_1 = 1.5$, $n_2 = 1.49$, $g = 2$) (a) 2D-image; (b) 1D-description.

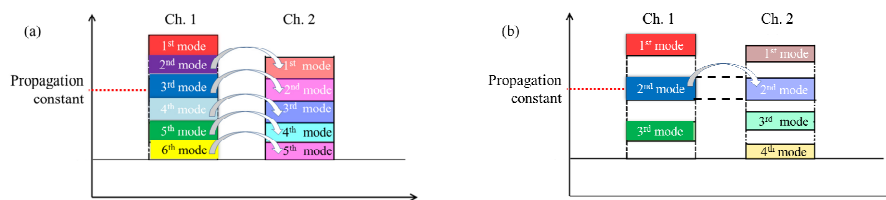


Fig. 3. The concept of mode coupling between multimode channels.(a) The continuous distribution; (b) The discrete distribution.

3. Relationships between inter-channel crosstalk and waveguide structure

3.1 Relationships between inter-channel crosstalk and core structure

For the numerical analysis of the propagating modes, we use the Beam Propagation Method (BPM). We focus on a 2-Ch. parallel waveguide (circular cores or square cores) characterized by Table 1, whose core-diameter (or width and height for square core) d is set to be $35.00 \mu\text{m}$, the core-index (n_1) and the clad-index (n_2) are set to be 1.5000 and 1.4900, respectively. Figure 4 shows the cross-section of the waveguide model for the simulation. For GI profiles in parallel cores, the refractive index profiles are approximated by utilizing the power-law approximation shown by Eqs. (4) and (5): The index exponent g is assumed to be 2.00. The inter-core pitch (Λ) is $45 \mu\text{m}$, and the waveguide length (L) is 10 cm. The incident beam is assumed to have a Gaussian intensity distribution whose spot size (beam waist) is $10 \mu\text{m}$, the NA is 0.1, and the wavelength is 850 nm. In order to validate the slow varying envelop approximation (SVEA) for BPM, the relative index difference between the cladding and outer medium should be less than the reference index of 1.5000. Hence, the refractive index of the outer medium is set to 1.4800, which is higher than that of air, but low enough compared to the refractive index of the cladding to confine the light in the cladding by total internal reflection. Hence, the tight confinement of the light in the cladding could increase the inter-channel crosstalk. In actual waveguides, even if they have no coating around their cladding, the waveguides could be integrated on a PCB, by which at least one surface is attached to a medium that could have a higher refractive index than that of the cladding. So, the actual waveguide claddings would confine the lightwave less tightly than the waveguide assumed to have a perfect boundary between the cladding and air. Hence, a rough surface model defined by Eq. (8) and Eq. (9) is introduced to the boundary between the cladding and the outer medium.

$$R(u) = \sigma^2 \exp[-|u|/D] \quad (8)$$

$$R(u) = \int h(z)h(z-u)dz \quad (9)$$

where, σ is the variance of the thickness and D is the correlation length. We add the difference function $h(z)$ to the cladding thickness (width and height).

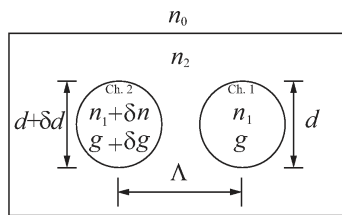


Fig. 4. Simulation model.

Table 1. Structural parameters

Waveguide length L	10.0 cm	Core-index n_1	1.5000
Core-pitch Λ	45.0 μm	Cladding-index n_2	1.4900
Core-size d	35.0 μm	Outer- index n_0	1.4800
Cladding-width W	130.0 μm	Index-exponent g	2.00
Cladding-height H	85.0 μm	The variance of the thickness σ	2.0 μm
		The correlation length D	1.0 μm

We vary the parameters of 1) difference in the core diameter (size) δd , 2) difference in the core index δn , and 3) difference in g parameter δg , between the two cores, and we compare the ratio of output powers from the launched core ($P_{Ch. 1}$) to the other core ($P_{Ch. 2}$), which is defined as the crosstalk, XT as described by Eq. (10):

$$XT = 10 \log_{10}(P_{Ch. 2} / P_{Ch. 1}) \quad (10)$$

Figures 5, 6, and 7 show the relationships between XT and the parameters of the core structural difference in the two cores defined above. It is found from Figs. 5–7 that the waveguide with the GI-type circular core is the most sensitive to structural changes. For example, only a 0.5 μm core size difference (δd) causes a 13-dB decrease in the crosstalk, while the crosstalk change in the other two cores is as small as 5 to 10 dB for the same core size differences, as shown in Fig. 6. As described previously, it could be due to the discrete distribution of propagation constants. Figure 8 shows the near-field patterns (NFPs) after a 10-cm propagation when δd is set to be 0 or 1 μm . When the two cores have the same structure, the output power from Ch. 2 (left hand side) is clearly observed in Figs. 8(a)–8(c), while the output power from Ch. 2 is the lowest in Fig. 8(d). These results also indicate that the difference in the distribution of propagation constant affects the inter-channel crosstalk.

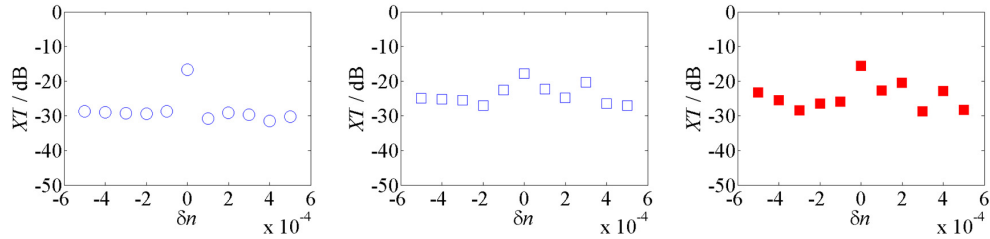


Fig. 5. Relationships between δn and XT (left: GI-circular, center: GI-square, right: SI-square).

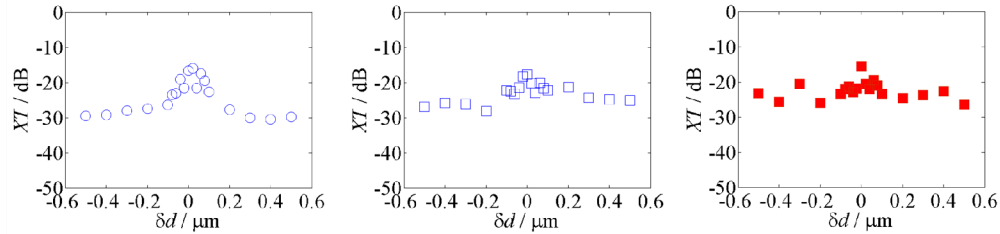


Fig. 6. Relationships between δd and XT (left: GI-circular, center: GI-square, right: SI-square).

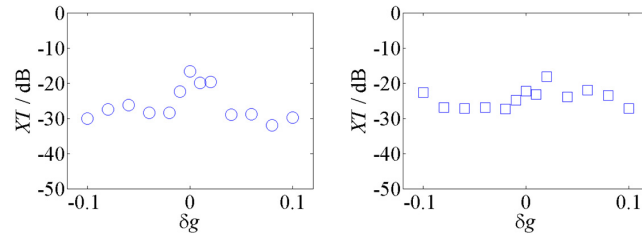


Fig. 7. Relationships between δg and XT (left: GI-circular, right: GI-square).

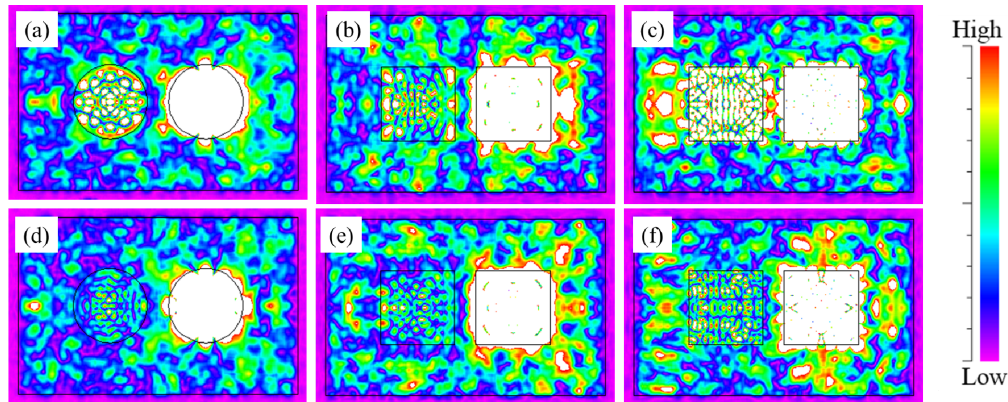


Fig. 8. Near-field pattern after a 10-cm propagation when Ch. 1 (right hand side) is excited. (a) GI-circular; (b) GI-square; (c) SI-square (two cores have the same core-index); (d) GI-circular; (e) GI-square; (f) SI-square (two cores have different core-indexes; δn is set to be 5.0×10^{-4}).

3.2 Relationships between inter-channel crosstalk and cladding mode

In the above section, we focused on the core structures and inter-channel crosstalk due to mode coupling. However, it is a concern that the light leaked from the launched core to the cladding could be confined in the cladding. The light leakage from the launched core could be due to the coupling loss at the input end, the leaky modes [11] in GI-type waveguides, or an excess scattering loss inherent to polymer materials. The cladding modes could possibly recouple to the other cores. Here, the crosstalk caused by the cladding mode is defined as the crosstalk due to “mode conversion.” Although the cladding modes attenuate severely due to the rough surface at the boundary of the cladding and outer medium, crosstalk due to mode conversion could already be involved in the results shown in Figs. 5–8. Meanwhile, Fig. 9 shows a cross-section of an experimentally fabricated 4-channel GI-type circular core waveguide when the signal light is coupled to one core (left edge core). It is found that the light from the launched core leaks to the cladding, while almost no optical output power is visually observed from the other three cores. There are several similar reports on such “dark cores” also in SI-core polymer waveguides [7]. Hence, we simulate the near-field patterns (NFPs) after transmission through 10-cm long waveguides when the same Gaussian beam as the one adopted in Section 3.1 is coupled not to the core but to the cladding deliberately. We apply the waveguide model in Table 2 to the analysis, where the two cores have identical structure and the inter-core pitch Λ is set to $85 \mu\text{m}$. In the simulation, the center of the Gaussian beam is projected at the point $10 \mu\text{m}$ displaced from the left edge of Ch. 2. At first, the boundary between the cladding and the outer medium is supposed to be a smooth surface, by which the cladding tightly confines the lightwave. Then, the light intensity distributions are compared. Figures 10(a)–10(c) show the calculated near-field patterns. On the other hand, Fig. 11 shows the calculated NFPs from a waveguide with rough outer surface of the cladding, where σ and D are set to be $1 \mu\text{m}$ and $2 \mu\text{m}$, respectively.

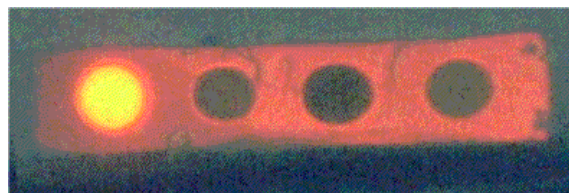


Fig. 9. Observed NFP from a GI-core polymer waveguide [3].

Table 2. Structural parameters

Waveguide length L	10.0 cm	Core-index n_1	1.50
Core-pitch Λ	85.0 μm	Cladding-index n_2	1.49
Core-size d	35.0 μm	Outer- index n_0	1.48
Cladding-width W	170.0 μm	Index-exponent g	2.0
Cladding-height H	85.0 μm		

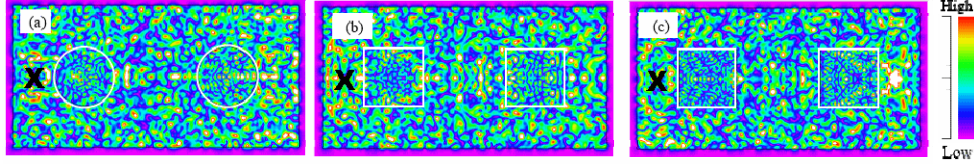


Fig. 10. NFP after a 10-cm waveguide propagation when the light is coupled to the cladding (A smooth boundary between the cladding and outer medium is assumed.) (a) GI-circular; b) GI-square; c) SI-square), X: injected point of Gaussian beam.

It is suggested that the output intensity from the two cores is almost equal to that from the surrounding cladding in Fig. 10.

On the other hand, by assuming the same rough-clad surface as the one adopted in Section 3.1, the optical confinement in the cladding decreases, as shown in Fig. 11.

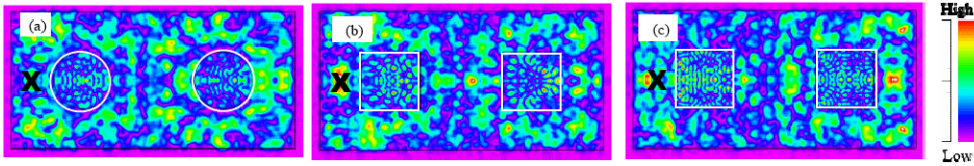


Fig. 11. NFP after a 10-cm waveguide propagation when the light is coupled to the cladding (A rough boundary between cladding-outer medium is assumed) (a) GI-circular; b) GI-square; c) SI-square), X: injected point of Gaussian beam.

Here, we compare the ratio of power density, p (average norm of Poynting vector; power per unit of area) between the core and cladding obtained by Eq. (11), and the results are summarized in Table 3.

$$C = \frac{\langle p_{core} \rangle}{\langle p_{cladding} \rangle} \quad (11)$$

Here, $\langle p_{core} \rangle$ and $\langle p_{cladding} \rangle$ are the average norm of the Poynting vector in the core and the cladding, respectively. Hence, $C = 1$ means the same output power is found the core as in the cladding.

Table 3. Ratio of averaged Poynting vector in core to cladding

Ratio of power density	Condition	GI-circular	GI-square	SI-square
C [a.u.]	Smooth surface	0.721	0.785	0.643
	Rough surface	0.551	0.698	0.967

As shown in Figs. 10 and 11, and Table 3, it is revealed that the power coupling efficiency (proportional to the crosstalk) from the cladding to the cores depends on the optical confinement in the cladding. That means if the cladding modes are attenuated by the outer medium (air or coating) due to the scattering at the rough surface or due to the absorption by

the coating materials, the output power from the unexcited cores decreases, resulting in dark cores particularly in the case of GI cores: the C value in Table 3 decreases. This could be due to the low power coupling between the cladding modes and the propagating modes. In addition, it is suggested that a GI-type circular core is a favorable structure for low crosstalk. This is because the coupled power is less likely to be observed than in GI-type square cores and SI-type square cores, not only caused by the mode coupling with the propagating modes in the adjacent cores but also caused by the cladding modes. In the case of SI-type square core waveguide, when a rough boundary exists between the cladding and the outer medium, the optical power leaked from the cladding to the outer medium is high compared to those in the GI-type circular and GI-type square cores. Hence, in the cases of GI-circular and GI-square cores, high optical power remained in the cladding allows the C value lower than 1 (dark core), while high power leakage from the cladding to the outer medium leads to the C value close to 1 in the case of SI-square core. The reason why the light leakage from the cladding is higher in the SI core should be investigated in more detail.

Here, we calculate the relationships between the crosstalk and the cladding thickness (called as cladding margin). The simulation model is shown in Fig. 12 and the parameters are summarized in Table 4.

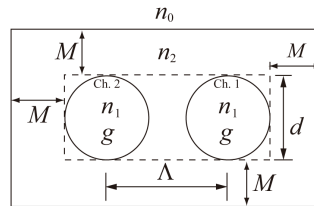


Fig. 12. Simulation model.

Table 4. Structural parameters

Waveguide length L	10.0 cm	Core-index n_1	1.5000
Core-pitch Λ	60-120 μm	Cladding-index n_2	1.4900
Core-size d	35.0 μm	Outer- index n_0	1.4800
Cladding-margin M	20-200 μm	Index-exponent g	2.00
The variance of the thickness σ	2.0 μm	The correlation length D	1.0 μm

We vary the parameters of the core-pitch Λ and the cladding-margin M . Figure 13 shows the relationships between the inter-channel crosstalk XT and the cladding margin M when the Gaussian beam same as the one adopted in section 3.1 is projected into Ch. 1.

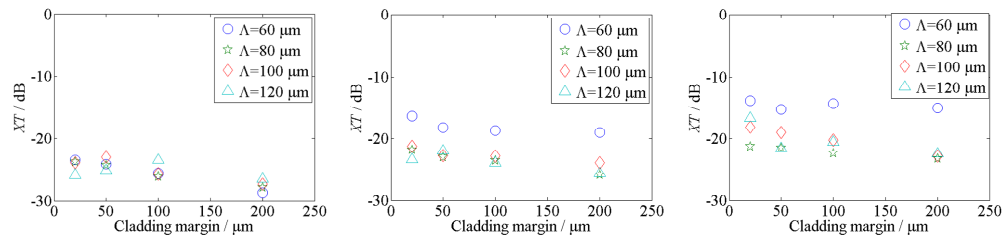


Fig. 13. Relationships between the cladding margin and XT (left: GI-circular, center: GI-square, right: SI-square).

As shown in Fig. 13, there is a tendency that the inter-channel crosstalk decreases with increasing the cladding margin. Only the crosstalk in the 60- μm pitch SI-square core is almost

independent of the cladding margin. This is because the crosstalk due to mode coupling is high in such a narrow pitch waveguide. Meanwhile, it is indicated that the inter-channel crosstalk in the waveguides with a pitch wider than $60\ \mu\text{m}$ is influenced by the cladding margin. This could be explained that the power density (the optical power per unit area) in the cladding increases with decreasing the cladding margin (the area of waveguide cross-section). Hence, when the pitch is sufficiently wide, a thin cladding (small cladding margin) can increase the inter-channel crosstalk. However, in this paper, we adopt a realistic value of cladding margin.

4. Inter-channel crosstalk analysis under actual measurement conditions

In this section, general experimental conditions for the measurement of inter-channel crosstalk are considered. In the actual measurements, the core is generally launched via an MMF probe, which could approximately fulfill the overfilled mode launch (OML) condition, while the output power from the waveguide core is coupled to another MMF probe for detection. Hence, we analyze the inter-channel crosstalk by taking the actual measurement conditions into account.

4.1 Mode coupling when launched via MMF

When the waveguide core is launched via an MMF, not only propagation modes but leaky modes could be excited. Hence, we compare the inter-channel crosstalk when launched via a $35\text{-}\mu\text{m}$ core MMF (GI or SI) almost attaining the OML condition, whose NA is set to be 0.2. For the analysis, we adopt the same waveguide model shown in Section 3.1, while σ and D are set to be $1\ \mu\text{m}$, and $2\ \mu\text{m}$, respectively, as well. The relationships between XT and the parameters of the core-index difference in the two cores are plotted in Fig. 14. Figure 15 shows the NFP when δn is set to be 0 and -5.0×10^{-4} .

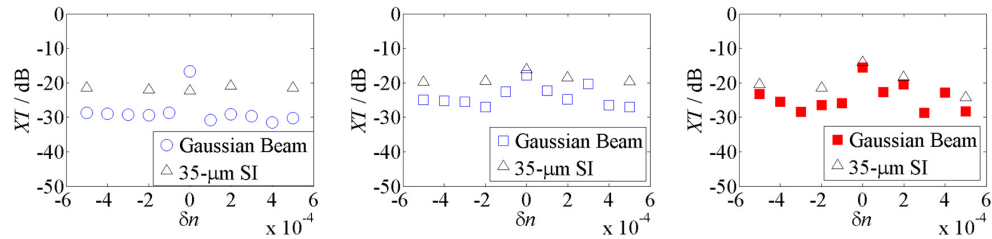


Fig. 14. Relationships between δn and XT (left: GI-circular, center: GI-square, right: SI-square).

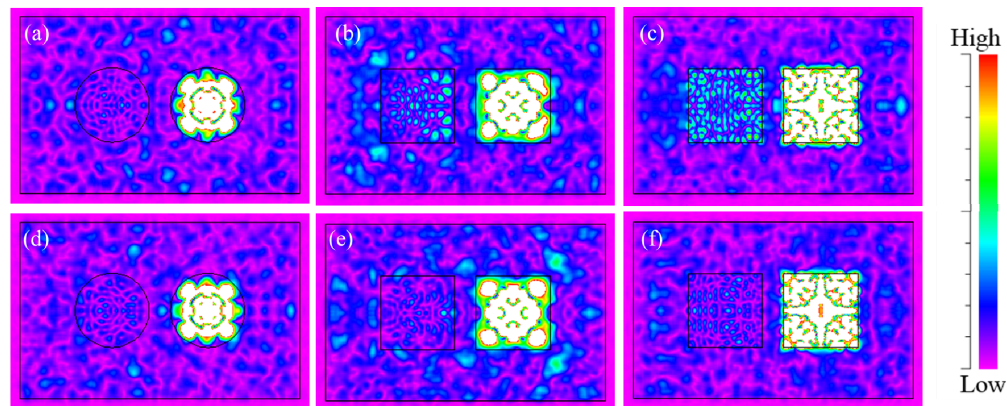


Fig. 15. Near-field pattern after a 10-cm propagation (a) GI-circular; (b) GI-square; (c) SI-square (two cores have the same core-index) (d) SI-circular; (e) GI-square; (f) SI-square (two cores have different core-index; δn is set to be -5.0×10^{-4}).

Table 5. Inter-channel crosstalk when the core is excited using 35- μm MMFs compared to the crosstalk when a Gaussian beam is injected

Launching condition		35- μm GI-MMF probe			35- μm SI-MMF probe			Gaussian Beam		
Waveguide		GI-circular	GI-square	SI-square	GI-circular	GI-square	SI-square	GI-circular	GI-square	SI-square
	δn									
Loss / dB	0.0	0.13	0.02	0.17	5.24	4.98	4.01	0.58	0.61	0.70
	-5.0×10^{-4}	0.05	0.03	0.15	5.22	4.98	3.91	0.50	0.58	0.64
χT / dB	0.0	-21.99	-19.51	-23.80	-22.28	-16.08	-14.12	-16.65	-17.80	-15.61
	-5.0×10^{-4}	-44.81	-22.82	-37.62	-21.43	-19.76	-20.45	-28.76	-24.96	-23.30

Figure 14 indicates that when the waveguide core is excited using a 35- μm core SI-MMF, the inter-channel crosstalk increases compared to the crosstalk excited by a Gaussian beam (Fig. 5), because the optical power leaked from the excited core is confined within the cladding. That means the crosstalk due to mode conversion increases. Therefore, under the actual measurement conditions, the different inter-channel crosstalk is observed among SI-square, GI-square, and GI-circular cores as shown in Figs. 14 and 15 due to the following two reasons: In terms of mode coupling, when structural difference exists in the two cores, the crosstalk in the GI-circular core is the lowest, as indicated in Figs. 5–7. Meanwhile, in terms of mode conversion, the optical power leaked from the excited core strongly affects the crosstalk. In some plots in Fig. 14, the crosstalk in the GI-circular core is higher than in the SI-square core when a 35- μm SI-MMF is used for the launch probe. This is attributed to high power in the cladding modes and the “leaky modes.” In GI-circular cores, the uncoupled power to the propagating modes at the input end is likely to couple to the “leaky modes” as well as the cladding modes, while the power of leaky modes are lower in the SI core and the GI-square core, due to the continuous distribution of the propagation constants. When the leaky modes are excited, the calculated coupling loss at the input end remains low, while the crosstalk increases due to the mode conversion from the leaky modes.

Table 5 shows the simulated relationship between the coupling loss at the input end of the waveguides and the crosstalk. When a 35- μm SI-MMF probe is used for launching the GI-type circular core, the optical loss is obviously high, because of the mode-field mismatch between the 35- μm SI-MMF probe and the GI circular core. So, high power remains in the cladding modes and even in the leaky modes, resulting in a crosstalk as high as -21.43 dB due to mode conversion.

Contrastingly, when a 35- μm GI-MMF is used for the launch probe, the coupling loss decreases although even high-order modes are sufficiently excited, resulting in obtaining a crosstalk as low as -44 dB for the GI-circular core. In the case of the GI-square core, the crosstalk due to mode coupling is essentially high, which is confirmed from the results under the 35- μm GI-MMF launch condition. The crosstalk between slightly different cores is as high as -22.82 dB despite very low coupling loss (0.03 dB) in Table 5. Hence, from the results in Table 5, we conclude that the GI-circular core exhibits the highest performance in the crosstalk.

Figure 16 shows the NFP, when a GI-MMF is used for the launch probe to excite the GI-type circular cores. This leads to the appearance of a “dark core.”

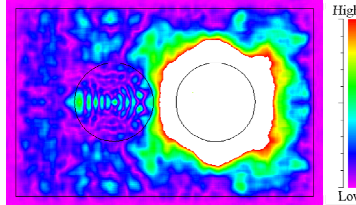


Fig. 16. Near-field pattern after a 10-cm propagation (GI-circular; two cores have different core-index).

Table 6 and Fig. 17 show the inter-channel crosstalk and the NFP when the inter-core pitch Λ is set to be $62.5 \mu\text{m}$ for the three core structures, respectively. When $\delta n = 0$ in Table 6, the calculated inter-channel crosstalk is mainly due to mode coupling. In these simulations, the same rough surface is assumed, and the same Gaussian beam is injected into the core. From Table 6, it is found that the crosstalk in GI-circular with a $62.5\text{-}\mu\text{m}$ pitch is insensitive to the structural difference in two cores, while in the GI-square and SI-square cores, the crosstalk largely decreases due to the structural difference. Compared to the narrow pitch ($45 \mu\text{m}$) waveguides shown in Fig. 5, the crosstalk due to mode coupling ($\delta n = 0$) is reduced due to the wider pitch. Furthermore, the crosstalk due to mode conversion also decreases because of the low power of the cladding modes. As Fig. 17 indicates, when we simulate the wider pitch waveguides, the cladding area needs to be expanded compared to the narrower pitch cases due to the wider pitch design. Therefore, even if the leaked power from the core is the same, namely same coupling loss, the power density in the cladding area decreases, resulting in decreasing the output power from the other core as crosstalk. Hence, it is suggested that the waveguide with GI-type circular core exhibits low inter-channel crosstalk.

Table 6. Inter-channel crosstalk when core-pitch is set to be $62.5 \mu\text{m}$

Core-pitch $\Lambda / \mu\text{m}$	δn	GI-circular	GI-square	SI-square
62.5	0.0	-30.6	-20.8	-21.8
	-5.0×10^{-4}	-30.8	-28.5	-26.6
45.0 (Fig. 5)	0.0	-16.7	-16.5	-14.2
	-5.0×10^{-4}	-28.8	-25.0	-23.3

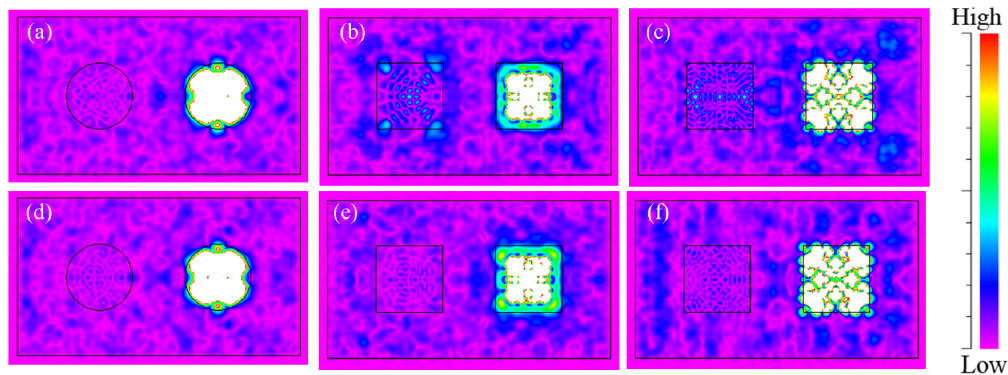


Fig. 17. Near-field pattern after a 10-cm propagation ($62.5\text{-}\mu\text{m}$ pitch) (a) GI-circular; (b) GI-square; (c) SI-square (two cores have the same core-index) (d) SI-circular; (e) GI-square; (f) SI-square (two cores have different core-indices; δn is set to be 5.0×10^{-4}).

5. Conclusion

We calculate the influence of the structural distortion in parallel cores of multimode waveguides on the inter-channel crosstalk by taking, mode coupling and mode conversion into account. It is revealed that the waveguide with GI-type circular cores exhibits low inter-channel crosstalk because the propagation constants of the propagation mode are discrete.